Journal of South American Earth Sciences 28 (2009) 345–359

Contents lists available at ScienceDirect

Journal of South American Earth Sciences

journal homepage: www.elsevier.com/locate/jsames

The Plutón Diorítico Moat: Mildly alkaline monzonitic magmatism in the Fuegian Andes of Argentina

M. González Guillot [a,*], M. Escayola [a], R. Acevedo [a], M. Pimentel [b], G. Seraphim [b], J. Proenza [c], I. Schalamuk [d]

[a] Centro Austral de Investigaciones Científicas (CADIC), CONICET, B. Houssay 200, 9410 Ushuaia, Argentina
[b] Instituto de Geociências, Universidade de Brasilia (UnB), 70910-900 Brasília, Brazil
[c] Departament de Cristalografia, Mineralogia i Depòsits Minerals, Facultat de Geologia, Universitat de Barcelona. Martí i Franquès s/n 08028 Barcelona, Spain
[d] Instituto de Recursos Minerales (INREMI)-UNLP and CONICET, La Plata, Argentina

ARTICLE INFO

Keywords:
Monzonitic magmatism
Fuegian Andes
Argentina

ABSTRACT

The Plutón Diorítico Moat (Moat Dioritic Pluton, PDM) is the largest of several isolated Cretaceous plutons exposed in the Fuegian Andes of Argentina. It is made of a large variety of rock types ranging from ultramafic bodies (pyroxenites and hornblendites) to syenites. The petrological diversity is thought to have been originated by fractional crystallization of a mantle-derived magma combined with minor assimilation of continental crust (AFC). Its geochemical characteristics indicate a mildly-alkaline monzonitic affinity, contrasting with the typical calc-alkaline plutons of the Southern Patagonian Batholith (PB) to the south, in the Chilean archipelago. The PDM original magma is arc-related and its crystallization, as indicated by the Rb–Sr mineral isochron age of 115 ± 3 Ma, is coeval with some plutons of the PB. Therefore a similar tectonic regime is assumed for the emplacement of these plutonic bodies, both south and north of the Beagle channel. Differences in magma sources and degree of partial melting are inferred to account for the contrasting lithological and geochemical characteristics of the PB and PDM. The data suggest that the original magmas of the PDM were generated at greater depths in the mantle, by a smaller degree of partial melting, compared with the PB. The Barros Arana basalts, exposed to the north in Chile, forming a back-arc volcanic complex, display the same mildly-alkaline shoshonitic affinity, and are considered in this study as the volcanic equivalents of the PDM. All the plutons in the Argentinean Fuegian Andes display similar lithological and geochemical characteristics and are, therefore, grouped in this work under the name of *Magmatismo Potásico Fueguino* (*Fuegian Potassic Magmatism*).

1. Introduction

In the southernmost tip of the Patagonian Andes, in the Argentinean Tierra del Fuego, small isolated Cretaceous plutons composed of a large variety of rock types, ranging from ultramafic to syenitic, are exposed. They have petrological and geochemical characteristics which contrast with the typical calc-alkaline nature of the rest of the plutonic rocks that constitute the Southern Patagonian Batholith (PB) of the Chilean Cordillera. The Plutón Diorítico Moat (PDM) is the largest of these bodies (25 km^2) and the one showing the best exposures.

The PDM encompasses the whole lithological spectrum from pyroxenite and hornblendite to syenite. Its major and trace element geochemical characteristics suggest that the original magmas were subduction-related and have monzonitic or shoshonitic affinity (Morrison, 1980; Fowler and Henney, 1996), with elevated contents of some of the LILE (Sr, K, Rb, Ba) and high K_2O/Na_2O (0.7–1.4) and LILE/HFSE ratios. The other plutons of Isla Grande show similar lithology and geochemistry (Acevedo et al., 2002, 2004; Cerredo et al., 2000, 2005). Additionally, these general geochemical characteristics are similar to those of the volcanic rocks of the Barros Arana Formation, which outcrop to the north, at 52°SL in Chile (Stern et al., 1991).

This study presents new petrologic, geochronologic and geochemical data on the largest exposure of plutonic rocks with mildly alkaline affinity of the Argentinean Fuegian Andes, which are named here the *Magmatismo Potásico Fueguino* (*Fuegian Potassic Magmatism*) (Fig. 1). This should be now interpreted as a unique rock association, clearly distinct from the PB, contradicting previous models, which considered both plutonic complexes as one single geological unit (Caminos, 1980; Caminos et al., 1981; Quartino et al., 1989; Acevedo, 1990, 1996; Acevedo et al., 1989, 2000, 2002, 2004; González Guillot et al., 2005).

* Corresponding author. Tel.: +54 2901 422310; fax: +54 2901 430644.
E-mail address: g_guillot@cadic.gov.ar (M. González Guillot).

0895-9811/$ - see front matter © 2009 Elsevier Ltd. All rights reserved.
doi:10.1016/j.jsames.2009.04.006

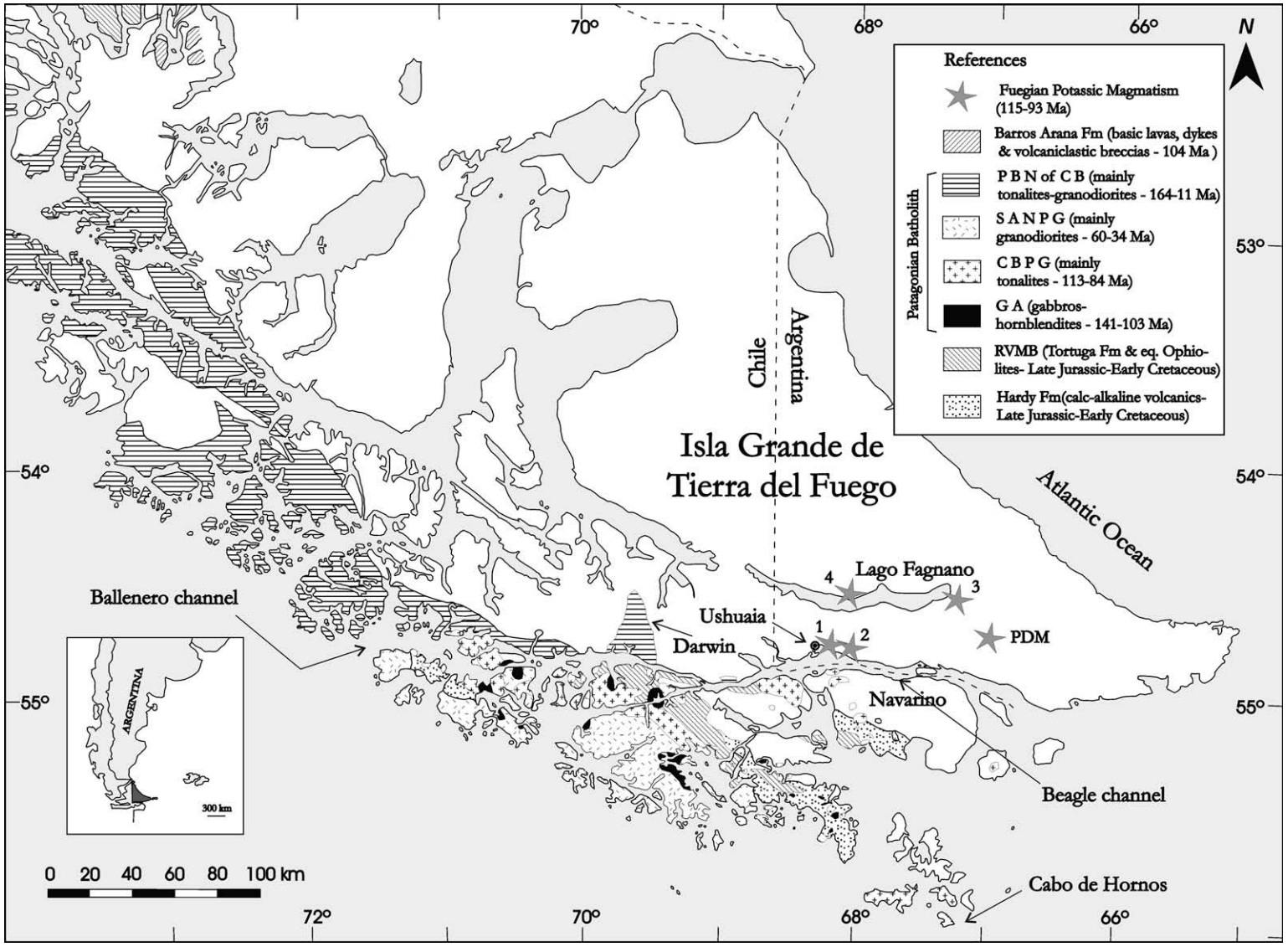

Fig. 1. Location of PB and the Fuegian Potassic Magmatism of Argentina. PDM: Plutón Diorítico Moat, other localities: 1: Hornblendita Ushuaia, 2: Trapecio hill, 3: Jeu-Jepén hill, 4: Kranck Mt. GA: Gabbroic Assemblage, CBPG: Canal Beagle Plutonic Group, SANPG: Seno Año Nuevo Plutonic Group, PBN of CB: Patagonian Batholith North of Beagle channel, RVMB: Rocas Verdes marginal basin. Data sources: Kranck, 1932; Suárez, 1978; Nelson et al., 1980; Hervé et al., 1984; Suárez et al., 1986; Stern et al., 1991; González Guillot et al., 2005. The subdivision of PB in the three groups GA, CBPG and SANPG (Hervé et al., 1984) has not been made North of Beagle or Ballenero channels.

2. Regional geology

During the Jurassic and Cretaceous an important igneous activity took place in the Fuegian Cordillera. A large volume of silicic volcanic rocks as well as minor basaltic flows (e.g. the Chon Aike LIP) were formed during an important extensional tectonic event. This is represented in the study area by the Middle-Late Jurassic Lemaire Formation (or Tobífera Formation, in Chile) formed mainly by rhyolitic to rhyodacitc lavas and ignimbrites, acidic breccias and tuffs, tuffaceous turbidites and slates. This important felsic magmatic event has been interpreted as the result of extensive melting of the continental crust (Bruhn et al., 1978; Féraud et al., 1999; Pankhurst et al., 2000; and references therein). The extensional regime eventually led to the development of the Rocas Verdes marginal basin (Katz, 1972, 1973; Dalziel et al., 1974) during Late Jurassic – Lower Cretaceous (Suárez, 1978). This resulted in the separation of a sliver of continental crust from the rest of the continent, where arc-related volcanism took place (Hardy Fm) in response to the subduction of the Pacific plate under the SW margin of Gondwana (Suárez, 1976, 1978; Bruhn et al., 1978).

The clastic infill of the marginal basin is represented by metapelites of the Yahgán Fm (Kranck, 1932; Katz, 1972; Dalziel et al., 1974; Suárez and Pettigrew, 1976; Winn and Dott, 1978).

Closure of the marginal basin and development of the fold and thrust belt occurred during the Late Cretaceous (Olivero and Martinioni, 1996; Fildani et al., 2003; Livermore et al., 2004). Intrusion of the Patagonian Batholith and the monzonitic plutons pre- and post-date this deformational event. Coeval with the monzonitic plutons, extrusion of basic lavas, dykes and volcaniclastic breccias of the Barros Arana Fm occurred (Soffia, 1988; Stern et al., 1991; Fig. 1). These interfinger with the upper stratigraphic levels of the Erezcano Fm (Tithonian-Albian), which is part of the sedimentary infill of the northern part of the basin. K–Ar analyses on amphibole megacrysts yielded the age of 104 ± 3 Ma (Stern et al., 1991). These lavas were interpreted by these authors as the mafic members of the mildly alkaline shoshonitic rock suite of the subduction-related arc.

The compressional deformation continued during the Cenozoic with migration of the fold and thrust belt towards the foreland. E–W trending transcurrent faults were tectonically active from mid-Cretaceous until the Present (Cunningham, 1993, 1995; Klepeis, 1994).

2.1. The Southern Patagonian Batholith

The Southern Patagonian Batholith (PB) is a multiple intrusion made of I-type metaluminous, calc-alkaline granitoids, distributed along a narrow belt parallel to the Pacific coast, from 47°SL to Cape Horn in Chile (56°SL). It consists mainly of tonalites and granodiorites (Suárez, 1977, 1978; Suárez et al., 1979, 1985a; Hervé, 1984; Hervé et al., 1984; Nelson et al., 1988). Magmatic activity that formed the PB took place almost continuously from ca. 152 to 11 Ma (SHRIMP U–Pb data on zircon; Bruce et al., 1991; Martin et al., 2001; Hervé et al., 2004), with a peak between 120 and 70 Ma (Bruce et al., 1991). In addition, scarce foliated S-type leucogranites, dated between ca. 164 and 157 Ma (Mukasa and Dalziel, 1996; Nelson et al., 1980), have also been described and are considered to be the plutonic equivalents of the Jurassic silicic volcanic rocks of the Lemaire Fm (Nelson et al., 1980).

Kranck (1932) divided the plutonic rocks of the Fuegian Cordillera into two groups: the "Central Cordillera Granites" which constitute the core of the Darwin Cordillera, and the "Andean Diorites" that outcrop in the Fuegian archipelago. More detailed work on the plutons exposed to the south of the Beagle channel (i.e. part of the "Andean Diorites" of Kranck) were carried out by Hervé et al. (1984). They described three plutonic groups (Fig. 1): (i) gabbroic assemblage (141–103 Ma, hornblende K–Ar), (ii) Canal Beagle Plutonic Group (113–84 Ma, hornblende K–Ar and biotite Rb–Sr ages, respectively) and (iii) Seno Año Nuevo Plutonic Group (60–34 Ma, biotite and hornblende K–Ar ages, respectively).

The Gabbroic Assemblage (GA) consists of gabbro, gabbronorite, hornblendite and diorite, exposed in isolated outcrops (up to 30 km^2) distributed along the batholith, as well as synmagmatic dykes or inclusions in the Canal Beagle Plutonic Group (Suárez et al., 1985b). The Canal Beagle Plutonic Group (CBPG) consists of tonalite, granodiorite and scarce quartz-monzodiorite. The granitoids show a penetrative synmagmatic foliation (Hervé et al., 1984; Suárez et al., 1985a). The Seno Año Nuevo Plutonic Group (SANPG) has similar composition but lacks the penetrative foliation that characterizes the latter group.

3. Local geology

The PDM is located in the Lucio López range in the Fuegian Andes (Isla Grande de Tierra del Fuego), 150 km east of Ushuaia (Fig. 1). This is an E-W trending range, composed basically of three supracrustal units: Lemaire, Yahgán and Beauvoir formations (Petersen, 1949; Caminos, 1980; Caminos et al., 1981; Olivero et al., 1999), intruded by the plutonic rocks of the PDM.

3.1. The Plutón Diorítico Moat

The PDM includes a main body composed of diorite-gabbro to monzonite, several minor apophysis, a small porphyritic stock to the NW, as well as small ultramafic bodies, all intruded into metasedimentary rocks of the Lemaire or Yahgán Formations (Fig. 2; González Guillot et al., 2005).

The ultramafic bodies comprise hornblendite and pyroxenite and form small (<700 m long) isolated outcrops. They are normally exposed along topographic lows, at the foothills of the mountain ranges. On the other hand, diorites–gabbros, monzodiorites–monzogabbros and monzonites form extensive outcrops, from the bottom of the valleys to the summit of the mountains. Monzonites outcrop basically at the SE end of the main body.

In some places the PDM displays a banded structure with alternating layers of hornblendite and gabbro (Fig. 3a and b; González Guillot et al., 2005).

Pyroxenites and hornblendites are coarse-grained (0.5–2 cm) cumulate rocks, and occasionally display coarser textures, forming pegmatitic pockets (Fig. 4a) in which the high volatile content favoured the development of hornblende crystals up to 30 cm long. They also frequently show irregular anorthosite or leucogabbro pockets, ranging in diameter from some centimeters to tens of centimeters. The development of these leucocratic portions was accompanied by brecciation of the enclosing ultramafic rock (Fig. 4b). Their mineralogy consists of hornblende, clinopyroxene, plagioclase and biotite. The crystallization order is given by an early paragenesis of pyroxene, apatite, opaques and plagioclase, followed by poikilitic hornblende enclosing the previously formed crystals. Finally, interstitial epidote of probable magmatic origin crystallized between the hornblende grains. Sphene occurs as a conspicuous accessory phase. The amount of plagioclase may be higher in some places, forming coarse-grained melagabbros. Partial replacement of pyroxene by hornblende is common, and both are also replaced partially by biotite. Opaque minerals form large (10–20 cm long) cumulus, spindle-shaped or sigmoidal. They consist of magnetite and ilmenite crystals associated with spinel, apatite, epidote and scarce chalcopyrite. Orthopyroxene and olivine were not found, nor pseudomorphs after them.

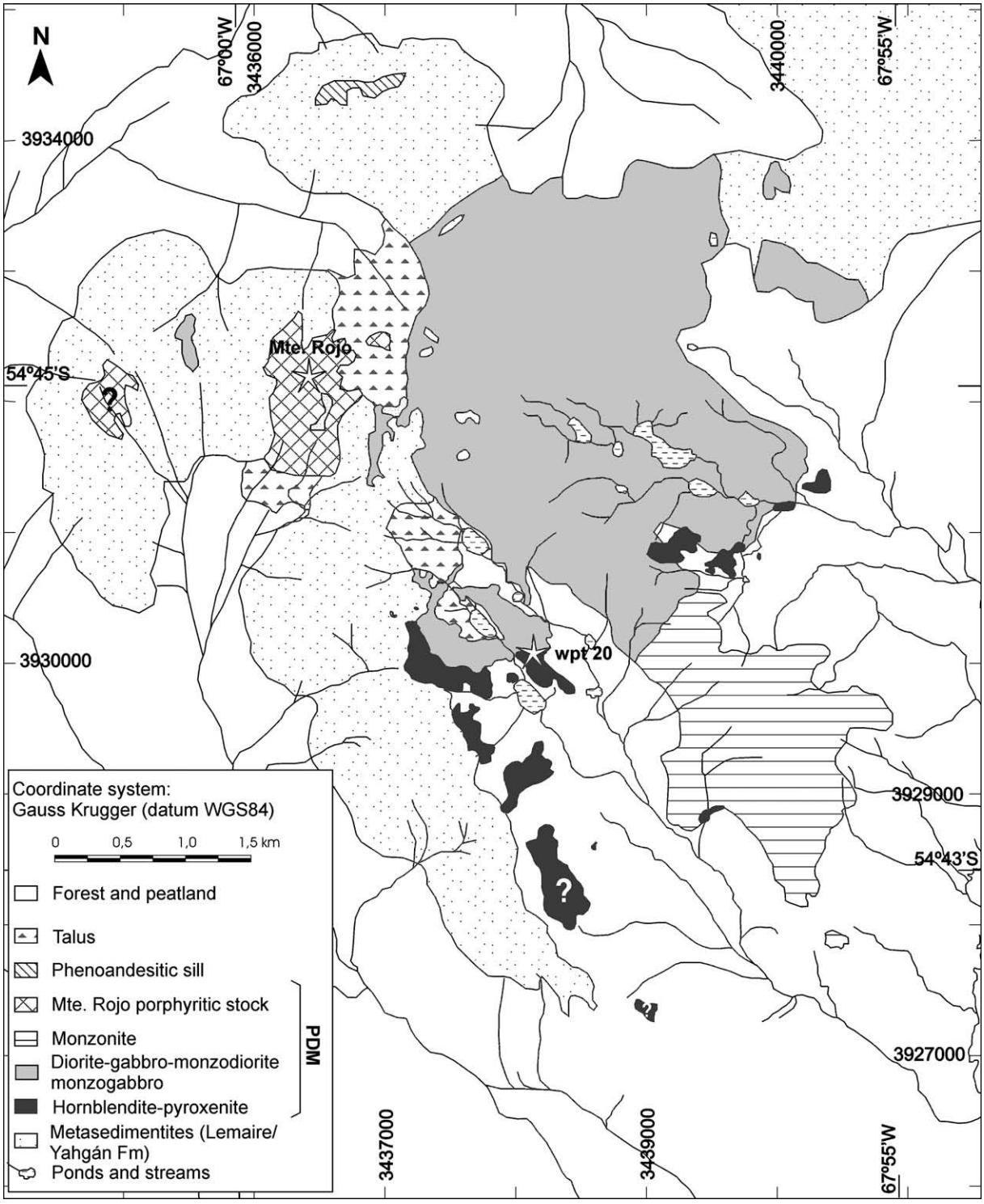

Fig. 2. Geologic map of PDM modified after González Guillot et al. (2005). The outcrops marked with (?) were not identified in the field. The rock composition range from diorite-gabbro to monzodiorite has the same pattern in this map. See Fig. 1 for location.

Diorites and gabbros are finer grained than the ultramafic rocks, presenting hypidiomorphic granular texture. In several places they show igneous layering (5–10 cm thick) formed by the alternation of light and dark layers due to variable contents of mafic minerals, grain size and texture (Fig. 4c). Additionally, it is common that these rocks display planar orientation of plagioclase and pyroxene crystals, defining a penetrative magmatic foliation, parallel to the igneous layering. The content of mafic minerals is variable, and melanocratic varieties are not uncommon. Similarly to the ultramafic rocks, in some diorites–gabbros pyroxene is more abundant, while in others, hornblende or biotite are dominant. Distribution of accessory phases is also uneven.

Elliptic hornblendite autoliths with sharp edges, arranged parallel to the magmatic foliation are abundant. The mineral composition is similar to that of the ultramafic rocks. Cumulus clinopyroxene and plagioclase crystallized first, followed by hornblende and biotite, forming the intercumulus phases.

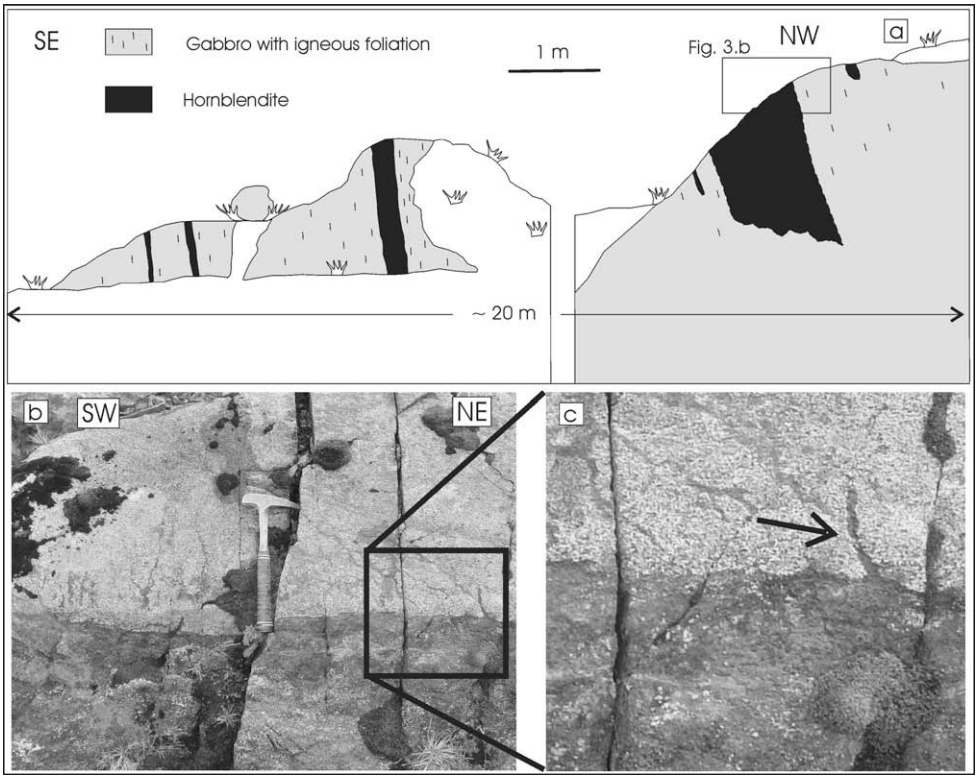

Fig. 3. (a) Schematic cross section showing igneous stratification between hornblendites and gabbro with igneous foliation parallel to strata. (b) Photograph showing the contact between the thickest hornblendite strata (darker) and gabbro in a. (c) Magnification of b. The arrow points to an injection of hornblendite into gabbro.

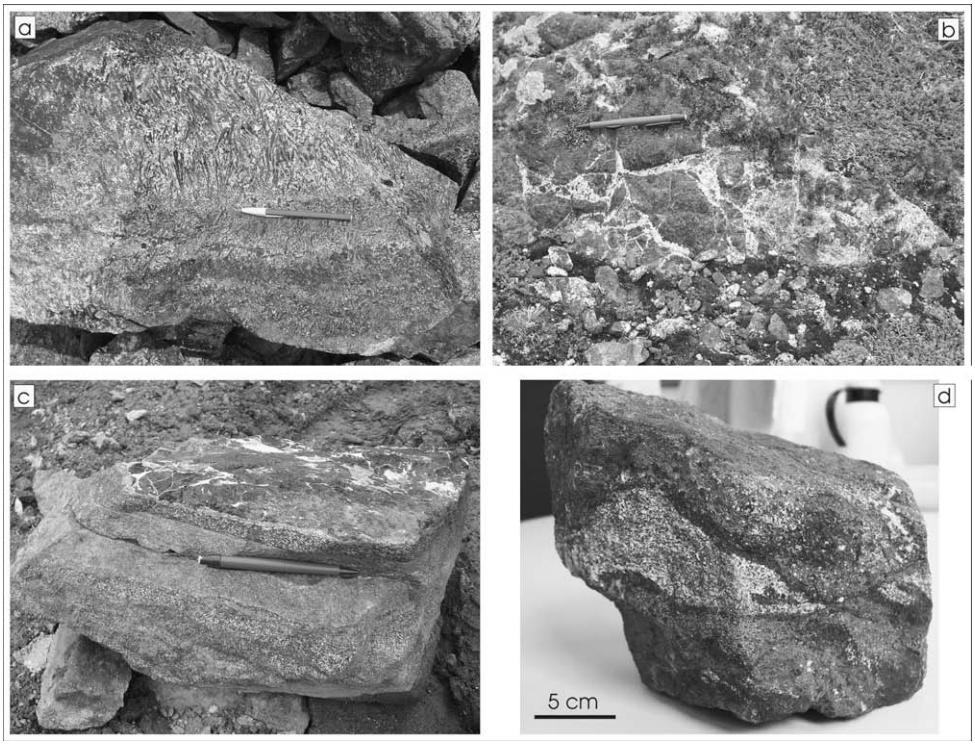

Fig. 4. (a) Pegmatitic pocket in hornblendite (note huge prisms of hornblende arranged in tooth-like texture). (b) Hornblendite brecciated by leucogabbro. (c) Igneous banding in gabbros and diorites (the upper band shows pegmatitic texture). (d) Deformed gabbro autolith in pyroxenite, with hornblende rim (dark rim).

The main difference between monzodiorites–monzogabbros–monzonites and the dioritic–gabbroic rocks is the presence, in the former, of anhedral interstitial crystals of more sodic plagioclase (untwinned), poikilitic and microperthitic alkali feldspar and scarce quartz. In monzonites, alkali feldspar develops coarser (up to 3 cm) and lesser poikilitic crystals with tendency to idio-

morphism. The interstitial phase is arranged in a consertal-like texture, with sutured edges, and causes embayments in the subhedral plagioclase crystals. The crystallization order is similar to that observed in diorites–gabbros, with the additional interstitial phases.

Plagioclase composition was investigated by electron microprobe. In a monzogabbro sample (CM7) subhedral plagioclase crystals are bytownite-labradorite (An_{76-52}), with normal zonation. In this sample there is no interstitial plagioclase, but alkali feldspar (Or_{92-87}) is present. Subhedral plagioclase from a monzonite sample (CM38) corresponds to andesine (An_{47-37}), also with a slight zonation. Interstitial plagioclase in the same rock shows a more sodic composition (An_{38-32}). This plagioclase is anhedral and fine grained, and precedes crystallization of the alkali feldspar. The latter shows slight zonation with increasing proportion of orthoclase molecules towards the edge (Or_{91-82}). Abrupt variations in the contents of mafic mineral or accessory phases are not common in monzonites. In this aspect, therefore, they are much more homogeneous than the diorites–gabbros.

Syenites occur as minor intrusions, forming discordant veins or segregations intruded into all the lithological groups described above. Vein thickness varies from 1 to 10 cm. Alkali feldspar forms large crystals (up to 4 cm), is microperthitic and has several inclusions of the other constituent minerals. Plagioclase is oligoclase (An_{21-14}) and display normal zonation, presenting an albite rim (Ab_{99-91}) wherever in contact with alkali feldspar. Other minor constituents are hornblende, biotite, sphene, zircon, quartz (always in contact with alkali feldspar) and magnetite.

Lamprophyric dykes are thin (1–20 cm thick), dark green, and cut all the rock types described above. They show porphyritic texture with aphanitic groundmass. Phenocrysts are hornblende ± pyroxene. The groundmass is composed of plagioclase laths, hornblende and pyroxene, and an interstitial leucocratic phase, which apparently consists of more sodic plagioclase often forming rims over plagioclase crystals. They contain rounded hornblendite autoliths. Contacts between dykes and host rock are sharp. Given its mineralogical composition they belong to the calc-alkaline lamprophyre group (spessartites).

At the Rojo Mt (Fig. 2) a small stock of 0.5×1.3 km^2 is exposed. It has characteristics that contrast with the rest of the pluton. It consists of red-coloured porphyritic diorites and monzonites. These rocks contain rounded hornblendite autoliths and are cut by syenite veinlets and lamprophyre dykes that constrain their age. Among its particular characteristics are porphyritic to microgranular texture, composition given mainly by leucocratic minerals (only 10–20% of mafic minerals) and abundant pyrite. Phenocrysts are 1–1.5 mm subhedral plagioclase showing strong multiple zonation (not seen in plagioclases of the rest of the pluton). Other phenocrysts, somewhat finer, are hornblende and pyroxene. Accessory phases are apatite and sphene.

Groundmass is aphanitic and consists basically of leucocratic and scarce mafic minerals.

A phenoandesitic sill was found intruded in the metasedimentary rock in the northern part of the area. It is composed of strongly zoned euhedral plagioclase phenocrysts, along with altered amphibole crystals. Groundmass is aphanitic consisting of felsic minerals. This rock contains abundant apatite as an accessory phase, as well as opaque minerals. Texture is glomeroporphyritic. It is similar to those outcropping at the Ushuaia peninsula (Hornblendita Ushuaia; Acevedo, 1990; Acevedo et al., 2002) and at Cerro Trapecio (unpubl. data).

3.2. Relationships among the different lithological types

Field observations (presence of autoliths and discordant veins) indicate the following order of emplacement of the different units of the PDM: pyroxenites and hornblendites → diorites–gabbros → monzodiorites–monzogabbros → monzonites → syenites → lamprophyres. Phenoandesitic sills exposed at the Ushuaia peninsula are cut by lamprophyres; thus the same temporal relationship is expected to occur here. Radiometric ages available in the literature for other intrusions in the area agree with the sequence of events aforementioned. This interpretation, however, in part contradicts the relationships described in previous studies (González Guillot et al., 2005) as well as for those observed in Cerro Jeu-Jepén (Fig. 1; Acevedo et al., 2000, 2004). These authors assume monzonite formation due to syenitic liquid percolation in diorites. An evolutionary process involving fractional crystallization (or AFC) with passage directly from dioritic to syenitic liquids is only possible if fractionation of cumulus phases takes place, as observed in the rocks investigated here. However, the composition of plagioclase and hornblende is different in monzonites and monzogabbros (microprobe analyses from diorites are lacking) from the PDM, which indicates that monzonites cannot represent contaminated diorites. Furthermore, the presence of large subhedral crystals of alkali feldspar in monzonites does not favour a model in which these rocks originated by syenite impregnation of diorites. Additionally, sharp contacts between monzonites and diorites have been recently found at Cerro Jeu-Jepén (unpubl. data). Hence, generation of monzonites after diorites by syenite impregnation is no longer feasible for this locality either.

In the sector called *wpt 20* (Fig. 2) the contact between hornblendites and gabbros occurs along a transition zone some tens of meters long. From SE to NW cumulus magnetite–ilmenite rich hornblendites, with progressive plagioclase enrichment towards the NW, pass into a zone of alternating parallel layers of hornblendite and foliated (magmatic) gabbro and, finally, into a zone dominated by foliated gabbros with elliptical hornblendite autoliths (Fig. 3a and b). The layers range from 1 m to 15 cm in thickness. Small ultramafic injections emanate from the hornblendite layers into the overlying gabbro–diorite, but not towards the underlying layer (Fig. 3c). This relationship requires that the gabbro layers were settled before complete crystallization of the underlying hornblendite layers, with the load pressure of the overlying gabbro expelling the interstitial hornblendite liquid upwards from the underlying layer rather than dykes intruding into the gabbros. González Guillot et al. (2005) interpreted this compositional variation as igneous layering of mafic and ultramafic cumulates, a phenomenon that also occurs within the gabbros–diorites elsewhere in the pluton (Fig. 4c). On the other hand, some diorite–gabbro autoliths in hornblendites and pyroxenites show minor strain, suggesting that mafic differentiates were not completely consolidated by the time they were incorporated into the ultramafic differentiates. These autoliths also have hornblende rims, which denote disequilibrium between both facies (Fig. 4d). These rims resemble ocellar textures where quartz grains are rimmed by mafic minerals and which are interpreted as the product of magma mixing (Vernon, 1990, 1991; Hibbard, 1991). Additionally, successive and irregular changes in lithology from pyroxenite-hornblendite to diorite–gabbro are commonly observed within small areas (dozens of meters) and are also suggestive of magma mixing-mingling processes.

All these characteristics expressed here suggest that mingling of magmas with varied composition was important in the least evolved PDM facies. It may result from the interaction of ultramafic and mafic magma currents in the chamber. During the activity of these currents (irrespective of whether acting simultaneously or acting on previous pulses not yet crystallized) one magma incorporates portions of the other. In more quiescent regimes, igneous layering formed by gravitational settling.

Near the contacts with the country rock, compositional and textural variations within the pluton have been observed, suggesting that some local metasomatic processes must have occurred due

to the interaction of the mafic magma with the country rock. In the case of diorites–monzodiorites a common feature, besides the smaller grain size, is the crystallization of biotite and quartz (the former in great quantities) along with abrupt decrease in hornblende and pyroxene. This phenomenon occurs in an aureole less than 10 m thick immediately adjacent to the contact with host rocks. Hornblendites and pyroxenites also show textural modifications close to the contact with the country rock, expressed by the development of large (~1 cm long) tabular poikilitic hornblende crystals.

4. Whole-rock geochemistry

Twelve samples covering the whole lithological spectrum of the PDM were analyzed for major and trace element contents (Table 1). In general, the geochemical data show similarities with the other plutons of the Argentinean side of Tierra del Fuego (see Acevedo et al., 1989, 2002, 2004; Cerredo et al., 2000, 2005) and significant differences when compared with the PB plutons. For comparative purposes with the PDM (and indirectly with the other intrusives of the area), contemporaneous PB plutons will be also included in the following discussion (i.e. GA and CBPG).

Chemical composition of PDM rocks varies from ultrabasic through intermediate (38–59.3% SiO_2) to acid (syenitic veins with 65.8% SiO_2). The most interesting geochemical feature is the alkaline trend depicted by these rocks, as displayed in the SiO_2 – $K_2O + Na_2O$ diagram, clearly contrasting with the calc-alkaline trend shown by the PB (Fig. 5a; González Guillot et al., 2005). Normative *Ne* in the CIPW norm for ultramafic and some mafic rocks also indicates this alkaline nature. A similar alkaline trend is proposed by Cerredo et al. (2000, 2005) for the Jeu-Jepén intrusive. Compared with the PB, the PDM displays distinctive enrichment in K_2O, with high K_2O/Na_2O ratio (>1 in the most evolved rocks), whereas in the GA and CBPG rocks this ratio is in the range between 0.24 and 0.35, respectively (Table 2). In the SiO_2–K_2O diagram (Fig. 5b) the PB rocks clearly define a medium-K calc-alkaline trend, whereas the PDM rocks plot in the shoshonite field (see also Cerredo et al., 2005).

Fig. 5 shows major element oxide plotted against SiO_2. CaO, MgO, Fe_2O_3t, TiO_2 and P_2O_5 (along with K_2O and total alkalis) de-

Table 1
Major and trace elements from PDM.

Sample	CM1[a]	CM3	CM4[a]	CM15	CM18	CM28	CM33	CM34[a]	CM36	CM37	CM38[a]	CM39
lithol.	px-hbt	gab	gab	hbt	mzd	gab*	RMtm	RMtm	sye	mzn	mzn	mzn
Wt%												
SiO_2	37.93	45.17	44.50	38.55	52.94	41.36	57.25	57.31	65.79	59.26	53.97	52.99
$Ti O_2$	1.92	1.13	1.14	1.59	0.67	0.71	0.41	0.42	0.07	0.40	0.75	0.62
Al_2O_3	10.67	18.07	17.86	17.12	18.95	21.80	19.56	19.77	18.90	19.27	16.90	19.20
Fe_2O_3t	20.09	12.59	12.86	13.18	8.52	8.48	4.84	3.93	0.97	4.20	8.44	7.65
MgO	11.93	4.95	5.05	9.33	2.88	4.12	1.23	1.00	0.08	1.03	3.64	2.41
MnO	0.20	0.25	0.25	0.18	0.19	0.16	0.18	0.14	0.02	0.15	0.17	0.20
CaO	14.50	11.46	12.78	13.19	8.16	16.97	6.31	6.01	0.98	3.95	7.13	7.87
Na_2O	1.15	2.62	2.35	1.61	3.78	1.64	5.25	5.03	4.17	4.70	3.09	3.57
K_2O	0.96	2.04	1.56	1.84	2.57	0.41	3.14	3.31	8.33	6.12	4.41	4.38
P_2O_5	0.15	0.82	0.86	1.30	0.5	0.95	0.25	0.26	0.02	0.19	0.46	0.46
LOI	0.30	0.70	0.40	2.0	0.70	3.20	1.40	2.20	0.90	0.70	0.60	0.40
Sum	99.82	99.81	99.62	99.90	99.87	99.80	99.82	99.38	100.23	99.97	99.56	99.76
K_2O/Na_2O	0.83	0.78	0.66	1.14	0.68	0.25	0.60	0.66	2.00	1.30	1.43	1.23
ppm												
Ba	121.2	566.6	522.8	389.4	540.4	78.3	922.3	990	161.3	622.3	716.5	1072
Hf	1.3	1.2	1.1	1.8	3.0	1.0	3.4	3.1	0.6	5.1	3.2	1.5
Nb	1.0	2.6	1.9	2.1	2.8	0.8	5.1	5.8	1.2	6.3	5.1	2.5
Rb	5.5	55.2	42.1	24.1	64	6.4	72.3	74.8	177.6	144.4	110	90.5
Sr	581.6	1629.2	1724.9	1122.0	1254.8	2109.4	1480.5	1569.5	441.9	1240.7	1433.9	2194.5
Ta	0.1	0.2	0.2	0.2	0.3	<0.1	0.6	0.4	0.2	0.7	0.5	0.2
Th	0.3	3.0	1.8	1.1	7.8	1.7	9.6	10.4	8.3	13.2	9.4	8.1
U	<.1	7.0	0.4	0.3	2.3	0.3	2.5	2.7	1.6	2.4	2.9	1.7
V	837.0	377.0	394.0	399.0	213.0	279.0	113.0	139.0	21.0	102.0	238.0	205.0
Zr	23.6	34.4	26.1	34.9	107.4	23.4	111.8	113.1	22.5	219.8	107.9	57.9
Y	18.4	23.9	25.1	26.2	19.4	16.9	21.6	22.1	2.9	20.9	23.5	19.9
Ni	33.0	17.0	5.0	10.0	11.0	5.0	5.0	5.0	5.0	5.0	17.0	8.0
Cr	13.68	34.21	13.68	20.53	27.37	13.68	13.68	6.84	20.53	20.53	27.37	20.53
ppm												
La	4.80	24.50	21.50	15.50	25.30	13.80	30.40	31.60	8.90	37.40	36,00	31.50
Ce	16.10	58.90	50,00	41.90	50.30	37.10	61.40	57.70	12.40	78.30	76.70	70.50
Pr	2.90	7.39	6.72	5.98	5.68	5.13	6.83	6.46	1.19	8.64	9.08	8.17
Nd	18.90	32.40	33.30	28.20	23.40	23.10	27,00	29,00	4.80	31.80	41,00	34.20
Sm	5.50	7.50	7.70	8.20	4.90	5.60	5.50	5.50	0.70	6.40	7.70	7.20
Eu	1.67	2.21	2.18	2.50	1.54	1.75	1.56	1.53	0.48	1.52	1.96	2.28
Gd	5.69	6.23	7.03	8,00	4.49	4.99	4.63	4.40	0.60	4.85	5.72	5.19
Tb	0.70	0.98	0.96	1.04	0.57	0.72	0.68	0.64	0.08	0.68	0.83	0.77
Dy	3.93	4.91	4.75	5.23	3.49	3.52	3.55	3.48	0.43	3.56	4.16	3.91
Ho	0.69	0.84	0.89	0.93	0.67	0.66	0.71	0.68	0.09	0.71	0.82	0.67
Er	1.65	2.21	2.30	2.31	1.90	1.54	2.04	2.05	0.24	2.08	2.17	1.80
Tm	0.22	0.33	0.33	0.29	0.30	0.22	0.31	0.33	0.06	0.36	0.35	0.32
Yb	1.45	2.35	2.14	2.10	1.73	1.45	2.17	2.21	0.32	2.30	2.05	1.95
Lu	0.19	0.31	0.29	0.29	0.36	0.19	0.31	0.33	0.04	0.31	0.29	0.25

Abbreviations: px-hbt: (pyroxene) hornblendite, gab: gabbro (*pegmatitic gabbro pocket in hornblendite with altered plagioclase), mzd: monzodiorite, R Mt m: Rojo Mt. monzonite, sye: syenite, mzn: monzonite.
[a] From González Guillot et al. (2005).

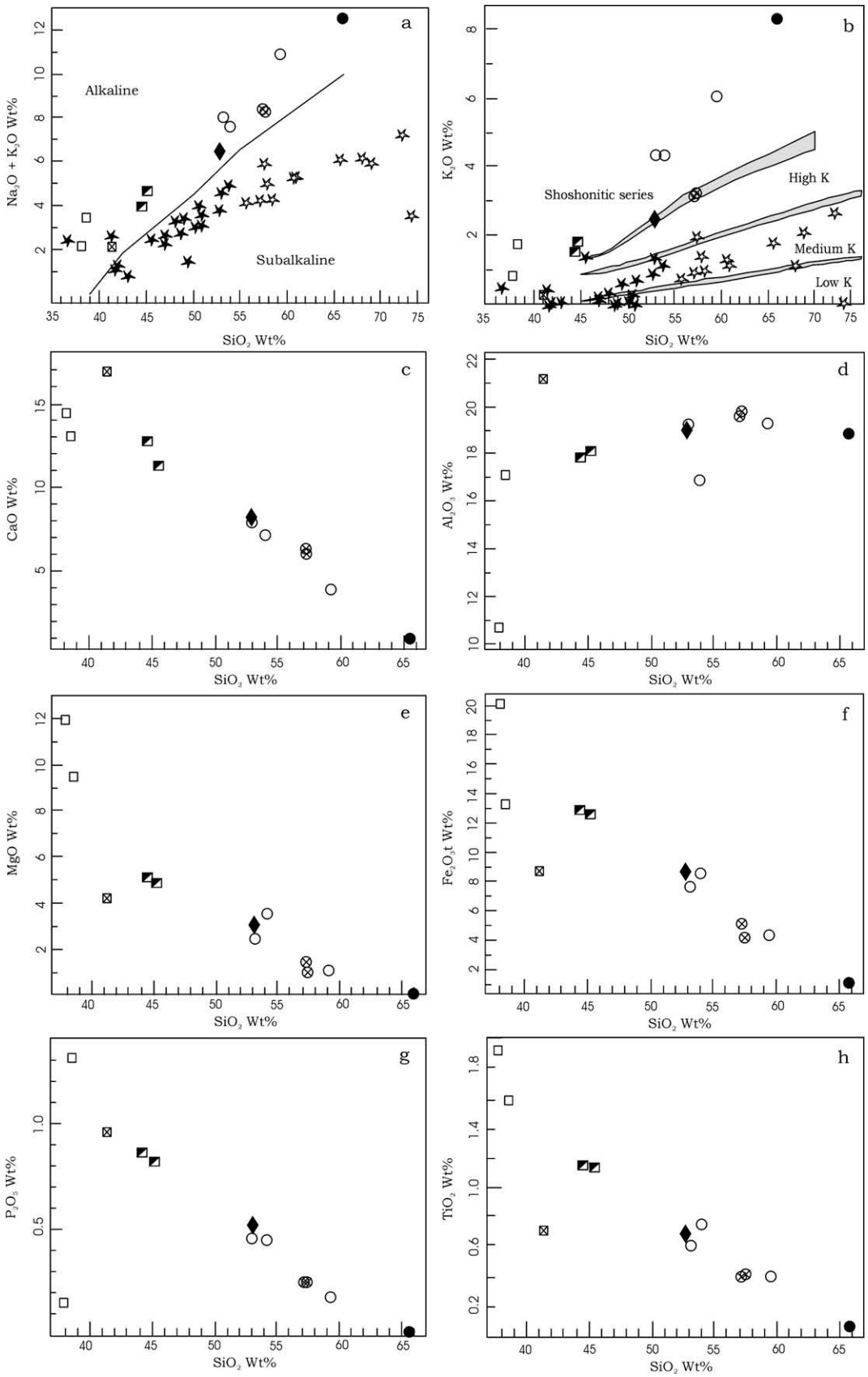

Fig. 5. (a)–(h) Harker diagrams from PDM. Open squares: hornblendite, crossed squares: leucogabbro pocket in hornblendite, half filled squares: gabbro, diamond: monzogabbro, open circles: monzonite, crossed circles: Rojo Mt monzonite, filled circle: syenite. Also in (a) and (b): solid stars: Gabbroic assemblage, open stars: Canal Beagle Plutonic Group (Hervé et al., 1984). Division(s) line(s) in (a) from MacDonald (1968), and (b) from Rickwood (1989).

Table 2
Trace elements and K_2O/Na_2O ratio from PDM and PB.

	Mean values						
	PDM			PB			
	hbt	gab	mz	dio	mz	to	gd
n	3	2	4	3	2	14	10
Ba (ppm)	196	545	811	239	800	305	496
Rb (ppm)	12	49	93	18	118	26	56
Sr (ppm)	1271	1677	1529	427	618	476	442
Zr (ppm)	27	30	120	71	212	113	136
Ce (ppm)	32	54	66	25	53	25	30.4
Rb/Zr	0.44	1.61	0.86	0.23	0.56	0.25	0.43
K_2O/Na_2O	0.74	0.72	1.16		0.24–0.35*		
(La/Y)N	3.43	5.81	9.30	4.90	11.21	6.64	7.33

Abbreviations: hbt: hornblendite, gab: gabbro, mz: monzodiorite – monzogabro monzonite (Rojo Mt monzonites were not considered), to: tonalite, gd: granodiorite. PB: Suárez, 1977, *CG and GPCB, respectively (Suárez et al., 1985c). Normalization factor for La/Y by Taylor and McLennan (1985). (*n*): number of samples.

fine continuous linear trends. In particular, TiO_2 and P_2O_5 display a negative trend without any break, emphasizing the early crystallization of apatite, sphene and ilmenite, which occurred continuously throughout the evolutionary history of the PDM.

Ba, Rb, Zr and Rb/Sr also show good continuous correlation with silica. The first two tend to replace K in alkali feldspar, so that its positive linear trend with respect to silica indicates the progressive crystallization of Kfs, especially from approximately 50% SiO_2 on (also seen in Fig. 5b).

Trace elements plotted in a spider diagram (Fig. 6a) show the typical spiked pattern, with Nb and Ta troughs, and K and Sr spikes that characterize subduction related magmas. For comparison purposes, trace element content from the PB (Suárez, 1977) is also shown. With respect to the PB (comparing equivalent lithologies), some LILE (Sr, K, Rb, Ba) enrichment and a greater LILE/HFSE ratio (as Rb/Zr indicates, Table 2) can be seen in the PDM.

Rare earth elements also show LREE enrichment with respect to HREE. Fig. 6b displays the fractionated REE pattern. Pyroxenites and hornblendites show a strong depletion in LREE, a trend that diminishes gradually towards the most evolved rocks. This can be due to the high content in hornblende (and to a lesser extent in clinopyroxene) of these rocks, since this mineral tends to incorporate MREE and HREE, so that LREE concentrates in the residual liquid. Additionally, ilmenite, an abundant phase in these ultramafic rocks, has very contrasting Kd values between the LREE and HREE, incorporating much less LREE with respect to HREE on the order of 6000:1 (Kd 0.000029 for La and 0.17 for Yb in alkaline basalts; Zack and Brumm, 1998).

5. Mineral chemistry

Microprobe analyses were carried out on the different lithological components of the PDM in order to characterize all mineral phases and to establish the physical parameters of crystallization.

Ferromagnesian silicate composition is of significant importance. Clinopyroxene belongs to the calcic pyroxene group (with a slight excess in the $CaSiO_3$ molecule), plotting in the diopside field in all lithological types (Fig. 7).

Hornblende shows two different compositional groups in the most and least evolved rocks (Fig. 8a and b). According to the classification of Leake et al. (1997), hornblende from the hornblendites, gabbros–diorites and monzogabbros plot in the magnesio-hastingsite field, whereas they correspond to magnesio-hornblende in monzonites and syenites.

Dzogolyk et al. (2003) present hornblende composition for granodiorites, monzodiorites and tonalites from the PB in Chile, between 50-52°SL. These data plot in the magnesio-hornblende field, comparable to the most evolved rocks of the PDM. Hornblende composition presented by Bruce et al. (1989) for an epidote-bearing diorite-gabbro corresponds to tschermakitic hornblende (Fig. 8b).

Amphibole displays alkali enrichment compared to the same minerals in the PB, with a K_2O content three times higher in the PDM than in the PB (Table 3).

Biotites are rich in MgO (11.1–13.6%; with Fe/(Fe + Mg) close to 0.5), although its content is not as high as in phlogopites (Fig. 8c, Table 3).

5.1. Geobarometry

Pressures were obtained using the method of Hammarstrom and Zen (1986) and the formula of Schmidt (1992), which is based on the Al content of hornblende in silica-saturated rocks. A trend of decreasing pressure with increasing differentiation was observed. The pressure intervals found are: 4.9–5.6 kbar for monzodiorites and monzogabbros, 3–3.6 kbar for monzonites and 1.4–1.5 kbar for syenite veins. Hornblendites do not match the geobarometer's

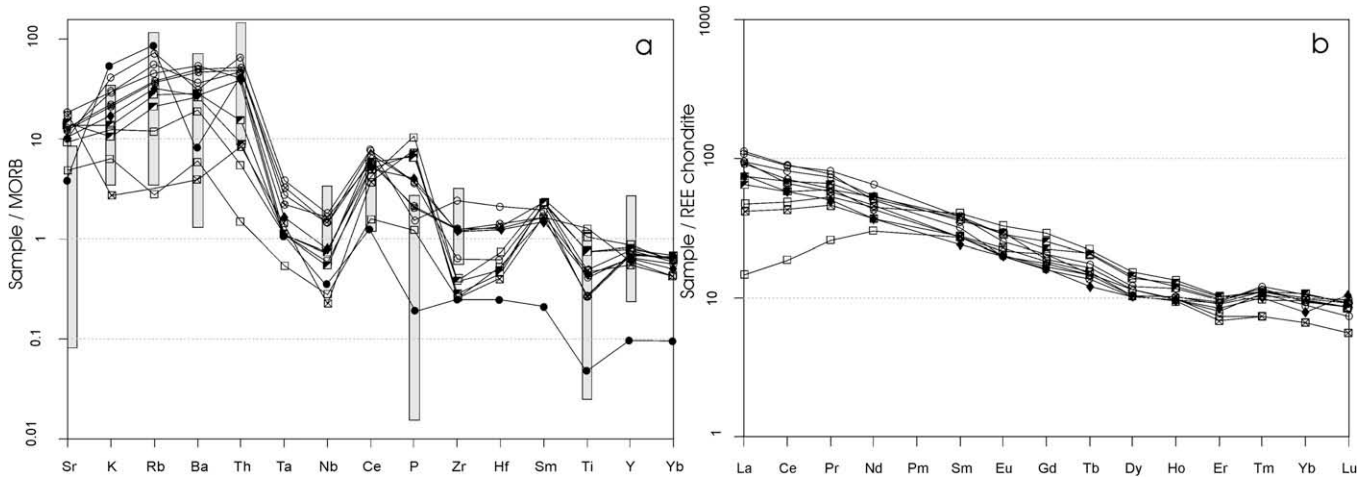

Fig. 6. (a) Trace multielement diagram from PDM. Normalization factor of Pearce (1983). (b) REE pattern from PDM. Normalization factor of Nakamura (1974). Same symbols as in Fig. 5. Bars in (a) represent PB south of Beagle channel (Suárez, 1977).

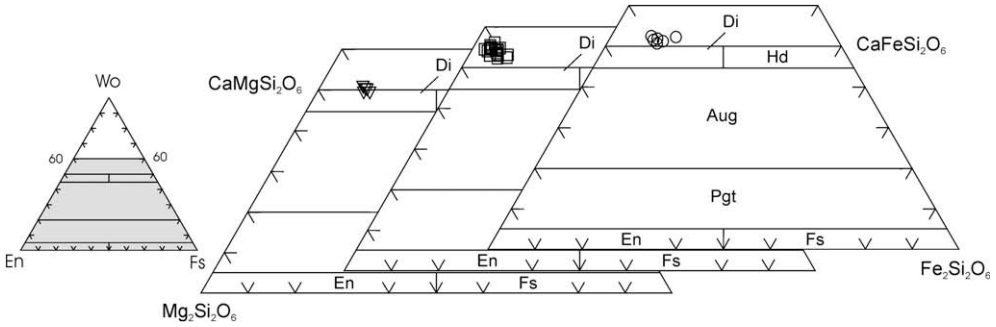

Fig. 7. Pyroxene classification after Morimoto (1988). Triangles: pyroxenite, squares: hornblendite, circles: monzonite.

requirements, but they contain magmatic epidote suggesting a crystallization pressure of 6–8 kbar, in agreement with Zen and Hammarstrom (1984).

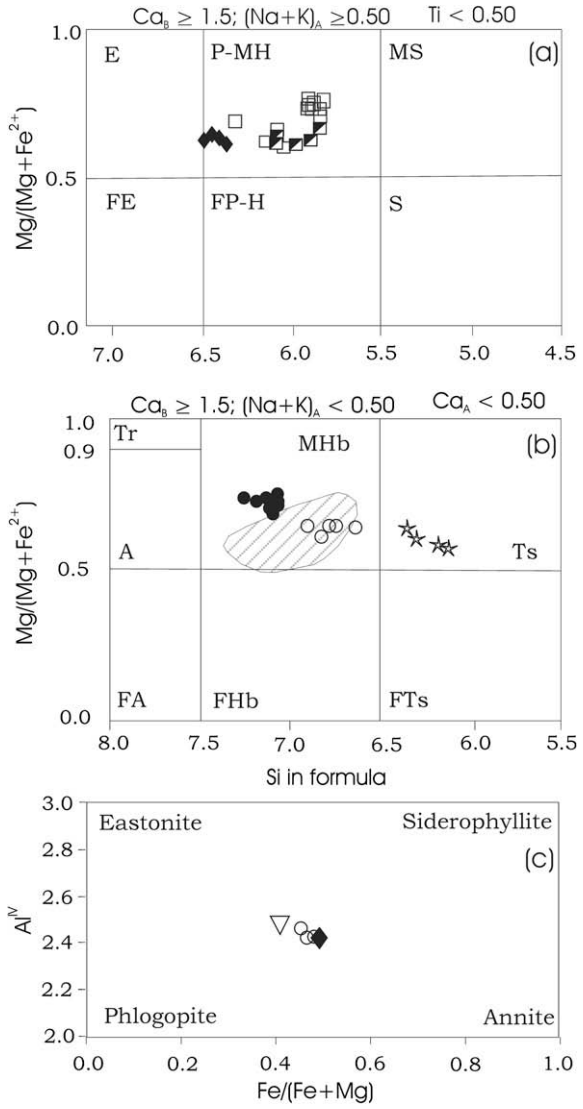

Fig. 8. Amphibole classification by Leake et al., 1997. (a) Open squares: hornblendite, half filled squares: sinmagmatic gabbro dyke (in hornblendite) and leucogabbro infill in brecciated hornblendite, diamond: monzogabro. They plot in the magnesio-hastingsite field (MH, with $Fe^{3+} > Al^{VI}$). (b) Open circles: monzonite, filled circles: syenite. Data plot in magnesio-hornblende field (MHb). Also for comparison data from PB: epidote bearing gabbro-diorite (stars; Bruce et al., 1989), monzodiorite, tonalite and granodiorite (striped field; Dzogolyk et al., 2003). (c) Biotite classification by Deer et al. (1966). Same symbols as above and as in Fig. 7.

6. Isotopic geochemistry

Nd isotopic data from the PDM are presented in Table 4. The $\varepsilon_{Nd}(110\ Ma)$ values range from +4.23 to −1.38. The highest values correspond to gabbros and hornblendites, while the lowest values belong to the most evolved rocks analyzed (monzogabbro and monzonite) as well as to a group of hornblendites with pegmatitic pockets rich in altered plagioclase (see above). Hornblendites have higher $^{147}Sm/^{144}Nd$ ratios, and these are progressively lower towards more evolved compositions. The $\varepsilon_{Nd}(t)$ values are roughly in the same range of those recently presented by Hervé et al. (2006) for the PB. According to these authors, the PB plutons show $\varepsilon_{Nd}(t)$ values progressively higher as age decreases. Values for plutons from the end of the Lower and Upper Cretaceous (122–77 Ma, an age interval which embraces that of the PDM) are +0.3 and +2.3, respectively; and Hervé et al. (2006) assume a lack of crustal involvement in plutons from that age on (until Neogene).

Nd isotopic data correlates well with variations in some trace and major element differentiation indicators; the progressive decrease in $\varepsilon_{Nd}(110\ Ma)$ values towards more evolved facies is accompanied, for example, by the increase in K_2O/Na_2O and $(La/Y)_N$ ratios, as well as in Rb, Zr and Ce contents. This does not favour differentiation of the original magmas in a closed system and calls for some degree of crustal contamination coeval with crystal fractionation. In such a model the most evolved rocks contain the highest proportion of crustal contaminant.

All samples analyzed (except CM4) yield Proterozoic T_{DM} ages. This could mean that the PDM rocks in part formed by melting of an old, possibly Grenville-age mantle or mafic-ultramafic composition lower crust, or, more likely, contamination of mantle-derived magmas with Proterozoic continental crust. Mesoproterozoic zircons were found by Hervé et al. (2003) in metasedimentary rocks from several complexes in the Patagonian Andes, which is consistent with incorporation of Grenville-aged crustal contaminants in the PDM magmas.

An initial $^{87}Sr/^{86}Sr$ (Sri) value (0.703906) was obtained from a coarse grained mafic rock from the PDM. This value is equivalent to the lowest $^{87}Sr/^{86}Sr$ values reported by Bruce et al. (1991) for the PB at 53°SL, which lie in the range between 0.7036 and 0.7050. These authors also indicate the progressive decrease in crustal involvement for granitoids, due to magmatic inflation, and propose that the diversity of lithological types within the PB is not related to assimilation processes. The exception to this are the S-type granitoids of the Darwin Cordillera (Upper Jurassic) with Sr isotope ratios greater than 0.7080 (Bruce et al., 1991). On the other hand, Weaver et al. (1990) established that crustal contribution has been significant in the PB at 48°SL, and that, similarly to the rest of the batholith, crustal assimilation decreases gradually with time. Sr and Nd isotopic values at 48°SL lie in the range between 0.7036 and 0.7074 and 0.51279–0.51217 (ε_{Nd} = 6.7 to −6), respectively (Weaver et al., 1988, 1990; Bruce et al., 1991).

Table 3
Composition of most abundant mafic minerals from PDM and PB.

cpx	PDM							BA	bt	PDM		
	CM19 pxt	CM1 px-hbt	CM25 hbt	CM25 dyke	CM41 l-g	CM41 pxt	CM38 mzn	Lava		CM19 pxt	CM7 mzg	CM38 mzn
Na_2O	0.29	0.33	0.41	0.65	0.51	0.24	0.45	0.15	Na_2O	0.14	0.07	0.04
K_2O	0	0	0.02	0	0	0	0.01	–	K_2O	9.01	8.88	8.71
TiO_2	0.21	0.73	0.2	0.47	0.49	0.87	0.14	0.59	TiO_2	4.19	3.53	3.15
MgO	13.8	13.3	13.7	12.4	12.8	13.5	12.7	14.6	MgO	13.60	11.10	12.33
Mg#	80	89	87	87	83	92	79	–	Mg#	59	51	53

hb	PDM							PB				BA
	CM1 px-hbt	CM25 hbt	CM25 dyke	CM41 l-g	CM7 mzg	CM38 mzn	CM36 sye	Epidote gabbro-dioirte				Lava
Na_2O	1.93	2.00	1.67	1.58	1.26	1.16	1.18	1.42	1.33	1.38	1.43	2.26
K_2O	1.67	1.45	1.67	1.45	1.28	0.79	0.47	0.59	0.57	0.55	0.57	1.79
TiO_2	2.07	1.97	2.35	1.97	1.57	1.01	0.58	0.55	0.63	0.74	0.34	2.71
MgO	13.1	11.8	11.1	11.0	11.0	12.0	13.8	8.6	9.2	9.8	8.3	11.5
Mg#	74	66	64	63	62	64	72	–	–	–	–	–

Abbreviations: pxt: pyroxenite, px-hbt: (pyroxene) hornblendite, dyke: syn-magmatic melagabbroic dyke, l-g: leucogabbro (breccia infill), mzn: monzonite, mzg: monzogabbro, sye: syenite. Data sources: PB: Bruce et al. (1989). Also data from Barros Arana Fm (BA; Stern et al. (1991), lava 7A), referred further, for comparison purposes.

Table 4
Sm and Nd isotopic data from PDM.

Sample	Lithol.	Sm (ppm)	Nd (ppm)	$^{147}Sm/^{144}Nd$	$^{143}Nd/^{144}Nd \pm 2SE$	$\varepsilon(0)$	$\varepsilon(t_{110})$	T_{dm} (Ga)
CM1	px hbt	5.38	17.26	0.1885	0.512794 ± 11	3.04	3.16	–
CM4	gab	7.3	33.155	0.1331	0.512809 ± 11	3.34	4.23	0.46
CM7	mzg	8.89	36.89	0.1456	0.51264 ± 11	0.03	0.76	0.9
CM13	gab*	1.554	7.588	0.1238	0.512531 ± 18	−2.09	−1.06	0.87
CM15	hbt	7.774	27.972	0.168	0.512744 ± 20	2.07	2.47	0.99
CM28	gab*	5.558	22.728	0.1478	0.512532 ± 8	−2.06	−1.38	1.17
CM38	mzn	7.738	38.51	0.1215	0.512574 ± 12	−1.24	−0.19	0.78

Abbreviations: px hbt: (pyroxene) hornblendite, gab: gabbro (* pegmatitic gabbro pocket in hornblendite with altered plagioclase), mzg: monzogabbro, mzn: monzonite.

7. Age

A Rb–Sr mineral isochron age (whole rock, hornblende, plagioclase) for a coarse-grained mafic rock of the PDM indicates an age of 115 ± 3 Ma. Other geochronological data present in literature (K–Ar whole rock) from equivalent plutons in Tierra del Fuego show that magmatic activity took place in the interval from 113 ± 5 to 86.9 ± 1.8 Ma (hornblendite, Acevedo et al., 2002; lamprophyre, Elsztein, 2004; respectively).

The geochronological record in Chile is much more abundant. As previously discussed, to the south of the Beagle channel, magmatic activity took place during three intervals corresponding to the plutonic groups described by Hervé et al. (1984); see above. According to this, igneous activity in the Argentinean Fuegian Andes was contemporaneous with the last pulses of the GA and the first ones of the CBPG.

8. Discussion

8.1. Evolution of the PDM

Variation diagrams of major and trace elements with respect to silica, especially CaO, MgO, Fe_2O_3t, TiO_2, K_2O (Fig. 5), Rb, Zr and Rb/Sr, show linear trends without gaps suggesting that the original PDM magmas evolved by continuous processes (FC or, most likely, AFC). The same patterns are depicted in the data from other plutons in the region (i.e. Hornblendita Ushuaia and Cerro Jeu-Jepén; Cerredo et al., 2000; Acevedo et al., 2002, 2004; and unpubl. data). The variability in the $^{143}Nd/^{144}Nd$ ratio within the PDM from 0.512809 ± 11 to 0.512531 ± 18, along with the scarce metasedimentary xenoliths present, and with the mineralogical changes that occur in the vicinities of the contacts with the host rock, as already mentioned, suggest that crustal contamination played a role during the evolution of the pluton. This participation of continental crust is more obvious in the most evolved rocks since they contain the metasedimentary enclaves and the lowest $^{143}Nd/^{144}Nd$ ratios.

On the other hand, as discussed above, there is also evidence for magma mingling between ultramafic and mafic rocks in the PDM. These pulses are probably generated by convective currents within the chamber, which mobilize magma portions of varied compositions, and, in the process, incorporate rock fragments from partially crystallized layers, which experience some ductile strain but do not completely mix. Both compositional end-members (ultramafic-mafic) do not show significant geochemical differences, except for those observed in the REE diagram (Fig. 6b), which may be explained by hornblende, clinopyroxene and ilmenite fractionation.

The low Ni and Cr contents (5–33 ppm and 13–116 ppm, respectively, for all the lithological spectrum, Table 1) indicate that these rocks represent differentiated mantle melts. The evolution of the PDM is, therefore, marked by important fractional crystallization of ferromagnesian silicates, plagioclase and Fe–Ti oxides resulting in a chamber with a cumulate floor of mingled ultramafic–mafic mush. Fractional crystallization was accompanied by some degree of crustal assimilation (AFC), resulting in a residual liquid showing progressive enrichment in alkalis and in crystallization of more sodic plagioclase and alkali feldspar. The conspicuous absence of olivine, along with the low contents of Ni and Cr in the rocks investigated, suggest that the rocks presently exposed at the surface are the products of previous magmatic differentiation of a primary magma, and that the least evolved end-members of the suite are not exposed or remain at greater depths.

This differentiation trend was carried out at different pressure intervals as indicated by the petrographic and geobarometric data. The ultramafic and mafic rocks crystallized at the highest pressure conditions (8–6 kbar) as suggested by the presence of magmatic epidote in some of these rocks, following the criteria of Zen and Hammarstrom (1984). Monzodiorites and monzogabbros crystallized at intermediate pressures (5.6–4.9 kbar), while monzonites and syenites solidified at the lowest pressure conditions (3–3.6 and 1.5–1.4 kbar, respectively). Bruce et al. (1989) found a similar trend of decreasing pressure in the different lithologies, from mafic to felsic, in the PB plutons. Since the different members of each pluton lie at the same crustal horizon, these authors deduced that the differences in depth obtained reflect important stages of uplift and erosion during magmatic activity, and that the depth of emplacement is a function of magma composition.

The ultramafic–mafic to felsic rock range of the PDM has also been emplaced in the same crustal level. In this case, the gradual decrease in pressure during lithological evolution not necessarily implies crystallization of liquids in shallower conditions, as the chamber was approaching the surface due to uplift and concomitant denudation of its cover. But the cause also could lie in a change from a (late-) compressional to extensional tectonic regime (and both criteria are not mutually exclusive). Radiometric ages of equivalent plutons in other localities of the Argentinean Fuegian Cordillera agree with this last hypothesis. Additionally, significant grain size changes in the rocks, from gabbros-diorites to syenites, have not been observed, which could imply progressive shallowing (except for the stock of Rojo Mt and the phenoandesitic sill).

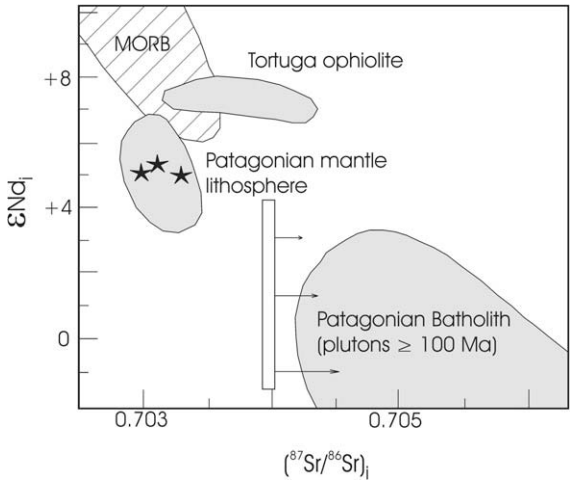

Fig. 9. Isotopic composition of PDM is shown schematically by a bar, since only one datum of $^{87}Sr/^{86}Sr$ is available. The bar encompasses the whole range of εNd_i data from PDM, located at 0.703906 $^{87}Sr/^{86}Sr$. The arrows depict the trend samples would supposedly take, assuming some crustal influence with the evolution of the pluton. This trend departs from the isotopic composition of the Patagonian mantle lithosphere (Stern et al., 1989, 1990), as well as of the Barros Arana Fm (stars, Stern et al., 1991). Data from Tortuga ophiolite (Stern, 1991), MORB (DePaolo, 1988) and ⩾100 Ma plutons of the Patagonian Batholith (Weaver et al., 1990) are also shown. Figure modified after Stern (1991).

8.2. The PDM vs. the PB

The data presented here show that crystallization of the PDM (and the other alkaline plutons of Tierra del Fuego) was coeval with the final stages of evolution of the Gabbroic Assemblage and with the initial magmatic pulses of the Canal Beagle Plutonic Group. The petrological and geochemical characteristics discussed in this work show significant differences when they are compared with those of the PB plutons, suggesting a different petrogenetic model for the PDM. The main differences are the absence of quartz, the K enrichment, the high K_2O/Na_2O ratio, along with a slight incompatible element enrichment, the higher LILE/HFSE and LREE/HREE ratios in the PDM (Table 2). These characteristics suggest the PDM has a mildly alkaline monzonitic affinity, contrasting with the typical calc-alkaline signature of the PB rocks. The least evolved rocks of the PDM could only be modally compared to the GA, but given these geochemical features and the evolution towards syenites of the former, it is clear that this similarity is only apparent and that significant differences in the genesis of the two magmas must have taken place to generate the suites to the south and north of Beagle channel.

This raises the question of why the PDM's geochemistry and range of lithologies differ from those of the PB. They both intruded at the same time and hence, probably reflect a similar tectonic regime. Therefore, the differences must reflect different magma sources and melting conditions, along with different degrees of continental crust assimilation. A long-lived subduction system can lead to a shift from calc-alkaline to K-rich, monzonitic or shoshonitic magmas. The latter magma types are commonly assumed to represent a transitional stage between calc-alkaline and alkaline magmas during late- and post-collisional evolution of a magmatic arc (Liegeois et al., 1998). There are two settings where such a

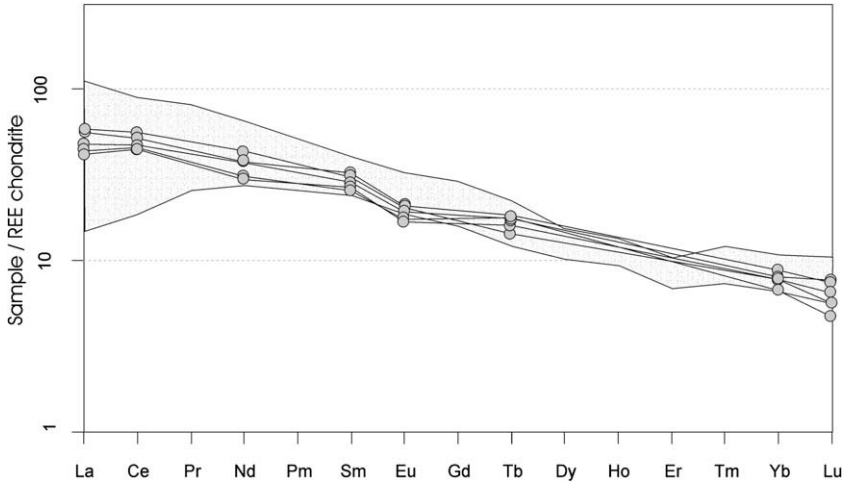

Fig. 10. REE patterns from PDM samples (stippled area) compared with those of Barros Arana Fm (gray circles) from Stern et al. (1991). Normalization factors by Nakamura (1974).

change is possible: firstly, once the descending oceanic slab has become dehydrated at depth, it loses its capacity to stimulate the generation of calc-alkaline magmas in the overlying mantle wedge, but it can still allow production of low degrees of partial melting, generating alkaline magmas at greater depths (K–h relationship of Dickinson (1975)), with significant volatile involvement to facilitate extraction of such low percentages of melt (McKenzie, 1985). Secondly, once subduction ceases, a stage of relaxation and uplift takes place, with generation of alkali-rich magmas (Fitton and Upton, 1987). This is not a viable alternative in the Beagle channel region since magmatism extended without interruption until 81 Ma (Suárez et al., 1985c). Several authors (Bailey, 1987; Thompson et al., 1989; Nelson, 1992; Gibson et al., 1993; Pitcher, 1993; Canning et al., 1996; Castro et al., 2003; among others) suggest that LILE enrichment of shoshonitic magmas comes from the mantle source itself, in a suprasubduction zone environment previously metasomatised by the recycling of sediments (Thompson and Fowler, 1986; Stille et al., 1989; Nelson, 1992).

The location of the outcrops with alkaline monzonitic affinity in Tierra del Fuego, in the back-arc region, far from the magmatic arc axis, suggests an environment where K and LILE enrichment either resulted from magma generation at greater mantle depths, characterized by low degrees of partial melting, or by contribution of an enriched lithospheric mantle. Involvement of crust as the chief agent of enrichment in the original magmas is discarded, since the least evolved rocks, which have the highest $^{143}Nd/^{144}Nd$ and lowest $^{87}Sr/^{86}Sr$ ratios (suggesting no crustal assimilation), also show high content in those elements. On the other hand, influence of lithospheric mantle on the enrichment in K and LILE would be negligible, since isotopic composition of the PDM is different from that introduced by Stern et al. (1989, 1990) for the southern Patagonian lithospheric mantle (Fig. 9). In summary, contamination with continental crust contributed to the differentiation of the magmas, but was not a fundamental process to explain the alkaline original nature of the PDM rocks; thus partial melting at greater mantle depths seems to be the most suitable mechanism.

The Barros Arana Fm (mafic lavas and dykes and volcaniclastic breccias; Soffia, 1988) is contemporaneous with the PDM and displays similar shoshonitic affinity. This igneous suite was also generated in the back-arc region, east of the Rocas Verdes ophiolites. It has a similar geochemistry, with enrichment in K and LILE and high LILE/HFSE and LREE/HREE ratios (Stern et al., 1991). Additionally, the composition of mafic minerals is also similar: Mg and Ca rich clinopyroxene (diopside) and hornblende (pargasite) with high alkali content (Table 3). The REE pattern is identical to that of PDM hornblendites and gabbros (Fig. 10). Based on these characteristics, we tentatively suggest that the Barros Arana Fm represents the volcanic equivalent of the PDM (and of other plutons in the region), although they considerably differ in isotopic composition (Fig. 9). The greater time of residence within the crust of the magmas that formed the PDM, compared to the Barros Arana basalts, could account for the higher $^{87}Sr/^{86}Sr$ ratios and lower $\varepsilon_{Nd}(t)$ values of the former, due to crustal assimilation (Fig. 9).

9. Conclusions

The PDM shows a silica-saturated trend (with low modal quartz content in the most evolved facies, i.e. from monzogabbros and monzodiorites on) with the alkali excess being accommodated in the mafic minerals (specially hornblende) with higher values in Na_2O and K_2O compared with the hornblendes of calc-alkaline rocks (Table 3). In addition, the abundance of hydrous mafic minerals (including biotite) reflects the enrichment in these oxides. Normative *Ne* appears in hornblendites and, to a lesser extent, in gabbros (from 6.35% to 0.33%).

All these characteristics may extend to the rest of the plutons of Isla Grande de Tierra del Fuego. For this reason, we propose the name of *Magmatismo Potásico Fueguino* (*Fuegian Potassic Magmatism*) with mildly alkaline affinity for all of them.

The lithological diversity of the PDM has been achieved by an evolution path involving continuous processes. The first crystallized products possibly accumulated at the bottom of the chamber by means of gravitational crystal settling or by magmatic currents suggested by the foliated gabbros and diorites. This cumulative process was oscillatory, producing layered structures. Several pulses of ultramafic and mafic differentiates, generated probably by convection within the chamber, have incorporated fragments of each other yielding structures typical of magma mingling. Rounded or spindle-shaped host rock enclaves are restricted to the most evolved facies, suggesting that assimilation of metasedimentary rocks had started at some point in the evolutionary trend towards monzonites and syenites. The isotopic composition variability between the most and least evolved rocks cannot be explained only by fractional crystallization; so AFC seems to be the most suitable evolutionary process that account for the observed features.

The mildly alkaline monzonitic character of the PDM, along with its lithological variability, suggests a separation from the PB. The location of the pluton in the rear of the arc far from the trench suggests a back-arc environment. Magmas were generated by the same subduction process that gives rise to the contemporaneous calc-alkaline plutons (GA and CBPG), but at greater mantle depths characterized by lower degrees of partial melting, according to the K–h relationship of Dickinson (1975). The normalized trace element pattern depicted by the PDM rocks (Fig. 6a) confirms that they are subduction-related, consistent with their plots in geotectonic discrimination diagrams. The Barros Arana Fm (contemporaneous shoshonitic series basalts) may represent the volcanic equivalent of the PDM. According to Stern et al. (1991), these rocks were deposited in a back-arc environment, during the initial stages of a slab flattening process. The low $^{87}Sr/^{86}Sr$ ratio and the high $\varepsilon_{Nd}(t)$ value of these basalts led Stern et al. (1991) to suggest an extensional back-arc environment at the moment of extrusion of the lavas (without crustal contamination). Meanwhile, a compressional regime prevailed at the arc axis. Soon after eruption of the Barros Arana basalts, a compressional regime installed in the back-arc region, which finally led to the closure of the marginal basin and migration of the magmatism towards the continent by late Albian. A compressional scenario is also thought to have existed to the south, north of the Beagle channel. The presence of pre- to late-tectonic contact metamorphic phases, subsequently overprinted by post-tectonic assemblages (unpubl. data), along with the geobarometric data, favour such an interpretation. This compressional regime permitted the settlement of magmatic chambers within the crust, with higher possibilities of assimilate crustal components and thus leading to an isotopic composition lower in $\varepsilon_{Nd}(t)$ and higher in $^{87}Sr/^{86}Sr$ for the PDM magmas with respect to Barros Arana basalts.

Acknowledgements

The authors want to thank Xavi Llovet from Universitat de Barcelona, for support with the microprobe analyses. We also thank Joan Reche (Universitat Autònoma de Barcelona) for his invaluable comments. Reviewers Guillermo Corretgé (Universidad de Oviedo) and Cees van Staal (Geological Survey of Canada) thoroughly contributed to enhance this paper. Mara Uría helped with translation into English. This work was financed by the Argentinean National Research Council (projects PIP CONICET 6535 and PICT 10-17348) and by the Brazilian National Research Council (project PROSUL/CNPq 490100/2003-1).

Appendix

Whole rock analyses were carried out at ACME Analytical Labs. Ltd., Canada, major elements by ICP-ES, and trace elements by ICP-MS. In both cases, 0.2 g samples were analyzed by $LiBO_2$ fusion and dilute nitric digestion.

Mineral compositions have been obtained by electron microprobe using a WDS CAMECA SX 50 instrument at the Serveis Cientificotècnics of the Universitat de Barcelona (Spain). Excitation voltage was 20 kV and beam current 15 nA. All the elements have been measured with counting time of 10 s. Minimum detection limit is 0.1 wt% for all the elements. Isotopic analyses were carried out at Laboratorio de Geocronología (Universidade de Brasília, Brazil) following the procedure of Goia and Pimentel (2000) for Sm–Nd measurements.

References

Acevedo, R.D., 1990. Destapes de cuerpos plutónicos ocultos en Península Ushuaia, Tierra del Fuego. In: XI Congreso Geológico Argentino, San Juan, Actas 1, pp. 153–156.

Acevedo, R.D., 1996. Los mecanismos sustitutivos y los factores de evolución en los anfíboles de la Hornblendita Ushuaia, Tierra del Fuego. Revista de la Asociación Geológica Argentina 51 (1), 69–77.

Acevedo, R.D., Quartino, G., Coto, C., 1989. La intrusión ultramáfica de Estancia Túnel y el significado de la presencia de biotita y granate en la Isla Grande de Tierra del Fuego. Acta Geológica Lilloana, San Miguel del Tucumán, Tomo XVII (1), 21–36.

Acevedo, R.D., Roig, C.E., Linares, E., Ostera, H.A., Valín-Alberdi, M.L., Queiroga-Mafra, J.M., 2000. La intrusión plutónica del Cerro Jeu-Jepén. Isla Grande de Tierra del Fuego, República Argentina. Cadernos do Laboratorio Xeolóxico de Laxe. A Coruña, España 25, 357–359.

Acevedo, R.D., Linares, E., Ostera, H.A., Valín-Alberdi, M.L., 2002. La Hornblendita Ushuaia (Tierra del Fuego): Geoquímica y Geocronología. Revista Asociación Geológica Argentina 57 (2), 133–142.

Acevedo, R.D., Roig, C., Valín-Alberdi, M.L., 2004. Lithologic types of the Jeu-Jepén Diorite. Isla Grande de Tierra del Fuego. In: Carcione, J., Donda, F., Lodolo, E. (Eds.), International Symposium on the Geology and Geophysics of the Southernmost Andes, the Scotia Arc and The Antarctic Peninsula (GeoSur). Buenos Aires, Argentina (Bolletino di Geofísica Teorica ed Applicata, 45(2), 113–117).

Bailey, D.K., 1987. Mantle metasomatism – Perspective and prospect. In: Fitton, J.G., Upton, B.G.J. (Eds.), Alkaline Igneous Rocks. Geological Society Special Publication No. 30. Blackwell Scientific Publications, pp. 1–13.

Bruce, R.M., Nelson, E.P., Weaver, S.G., 1989. Effects of synchronous uplift and intrusion during magmatic arc construction. Tectonophysics 161, 317–329.

Bruce, R.M., Nelson, E.P., Weaver, S.G., Lux, D.R., 1991. Temporal and spatial variations in the Southern Patagonian Batholith, constraints on magmatic arc development. In: Harmon, R.S., Rapela, C.W. (Eds.), Andean Magmatism and its tectonic setting. Geological Society of America Special Paper 265. Boulder, Colorado, pp. 1–12.

Bruhn, R.L., Stern, C.R., De Wit, M.J., 1978. Field and geochemical data bearing on the development of a Mesozoic volcano-tectonic rift zone and back-arc basin in southernmost South America. Earth and Planetary Science Letters 41 (1), 32–46.

Caminos, R., 1980. Cordillera Fueguina. Geología Regional Argentina, Vol. II. Academia Nacional de Ciencias, Córdoba. pp. 1463–1501.

Caminos, R., Haller, M., Lapido, O., Lizuain, A., Page, R., Ramos, V., 1981. Reconocimiento geológico de los Andes Fueguinos. Territorio Nacional de Tierra del Fuego. In: VIII Congreso Geológico Argentino San Luis, Actas 3, pp. 754–786.

Canning, J.C., Henney, P.J., Morrison, M.A., Gaskarth, J.W., 1996. Geochemistry of late Caledonian minettes from northern Britain: implications for the Caledonian sub-continental lithospheric mantle. Mineralogical Magazine 60, 221–236.

Castro, A., Corretgé, L.G., De La Rosa, J.D., Fernández, C., López, S., García Moreno, O., Chacón, H., 2003. The appinite-migmatite complex of Sanabria, NW Iberian Massif, Spain. Journal of Petrology 44, 1309–1344.

Cerredo, M.E., Tassone, A., Coren, F., Lodolo, E., Lippai, H., 2000. Postorogenic, alkaline magmatism in the Fuegian Andes: the Hewhoepen intrusive (Tierra del Fuego Island). In: IX Congreso Geológico Chileno, Puerto Varas, Actas 2, Simposio Nacional 2, pp. 192–196.

Cerredo, M.E., Remesal, M.B., Tassone, A., Lippai, H., 2005. The shoshonitic suite of Hewhoepen pluton, Tierra del Fuego, Argentina. In: XVI Congreso Geológico Argentino, La Plata, Actas I, pp. 539–544.

Cunningham, W.D., 1993. Strike-slip faults in the southernmost Andes and the development of the Patagonian orocline. Tectonics 12, l69–186.

Cunningham, W.D., 1995. Orogenesis at the southern tip of the Americas: The structural evolution of the Cordillera Darwin metamorphic complex, southernmost Chile. Tectonophysics 244, 197–229.

Dalziel, I.W.D., de Wit, M.F., Palmer, K.F., 1974. Fossil marginal basin in the southern Andes. Nature 250, 291–294.

Deer, W.A., Howie, R.A., Zussman, J., 1966. An Introduction of the Rock Forming Minerals. Harlow, Longman. 528p.

DePaolo, D.J., 1988. Neodymium isotope geochemistry. Minerals and Rocks, 20. Springer Verlag. 187p.

Dickinson, W.R., 1975. Potash-Depth (K-h) relations in continental margin and intra-oceanic magmatic arcs. Geology 3, 53–56.

Dzogolyk, E., Hervé, F., Belmar, M. 2003. Termobarometría de Al en hornblenda en el Batolito Surpatagónico, entre los 50° y 52° Latitud Sur. In: X Congreso Geológico Chileno, Concepción (Actas in CD).

Elsztein, C., 2004. Geología y evolución del Complejo Intrusivo de la Península Ushuaia, Tierra del Fuego. Undergraduate Thesis (unpublished). Facultad de Ciencias Exactas y Naturales, Universidad de Buenos Aires, 103p.

Féraud, G., Alric, V., Fornari, M., Bertrand, H., Haller, M., 1999. 40Ar/39Ar dating of the Jurassic volcanic province of Patagonia: migrating magmatism related to Gondwana break-up and subduction. Earth and Planetary Science Letters 79, 83–96.

Fildani, A., Cope, T.D., Graham, S.A., Wooden, J.L., 2003. Initiation of the Magallanes foreland basin: Timing of the southernmost Patagonian Andes orogeny revised by detrital zircon provenance analysis. Geology 31 (12), 1081–1084.

Fitton, J.G., Upton, G.J., 1987. Introduction. In: Fitton, J.G., Upton, G.J. (Eds.), Alkaline Igneous Rocks, Geological Society Special Publication No. 30. Blackwell Scientific Publications.

Fowler, M.B., Henney, P.J., 1996. Mixed Caledonian appinite magmas: implication for lamprophyre fractionation and high Ba–Sr granite genesis. Contributions to Mineralogy and Petrology 126, 199–215.

Gibson, S.A., Thompson, R.N., Leat, P.T., Morrison, M.A., Hendry, G.L., Dickin, A.P., Mitchell, J.G., 1993. Ultrapotassic magmas along the flanks of the Oligo-Miocene Rio Grande rift, USA: monitors of the zone of lithospheric mantle extension and thinning beneath a continental rift. Journal of Petrology 34, 187–228.

Goia, S.M., Pimentel, M., 2000. The Sm-Nd isotopic method in the Geochronology Laboratory of the University of Brasilia. Annals Academia Brasileira de Ciencias 72, 219–245.

González Guillot, M., Seraphim, G., Acevedo, R.D., Escayola, M., Schalamuk, I., Pimentel, M., 2005. El Plutón Diorítico Moat: una nueva manifestación del Batolito Patagónico Austral en la provincia de Tierra del Fuego, Argentina. In: XVI Congreso Geológico Argentino, La Plata, Actas I, pp. 627–634.

Hammarstrom, J.M., Zen, E-an, 1986. Aluminium in hornblende: An empirical igneous geobarometer. American Mineralogist 71, 1297–1313.

Hervé, M., 1984. Rb–Sr and K–Ar geochronology of the Patagonian Batholith, south of the Beagle and Ballenero channels and west of Long. 68 degrees 00', Master's Thesis, University of Texas at Dallas, Richardson, TX, United States, 53p.

Hervé, M., Suárez, M., Puig, A., 1984. The Patagonian Batholith south of Tierra del Fuego, Chile. Timing and tectonic implications. Geological Society of London Bulletin 141 (5), 909–917.

Hervé, F., Fanning, C.M., Pankhurst, R.J., 2003. Detrital zircon age patterns and provenance of the metamorphic complexes of southern Chile. Journal of South American Earth Sciences 16, 107–123.

Hervé, F., Godoy, E., Mpodozis, C., Fanning, M., 2004. Monitoring magmatism of the Patagonian Batholith through the U-Pb SHRIMP dating of detrital zircons in sedimentary units of the Magallanes Basin. In: Carcione, J., Donda, F., Lodolo, E. (Eds.), International Symposium on the Geology and Geophysics of the Southernmost Andes, the Scotia Arc and The Antarctic Peninsula (GeoSur). Buenos Aires, Argentina (Bolletino di Geofísica Teorica ed Applicata, 45(2), 113–117).

Hervé, F., Pankhurst, R.J., Fanning, C.M., Calderón, M., 2006. The South Patagonian batholith: 150 Ma of magmatism at a plate edge. Backbone of the Americas: Patagonia to Alaska, GSA Specialty Meetings, Abstracts with Programs, No. 2, p. 119.

Hibbard, M.J., 1991. Textural anatomy of twelve magma-mixed granitoid systems. In: Didier, J., Barbarin, B. (Eds.), Enclaves and Granite Petrology. Developments in Petrology, vol. 13. Elsevier, pp. 431–444.

Katz, H.R., 1972. Plate tectonics and orogenic belts in the south-east Pacific. Nature 237, 331–332.

Katz, H.R., 1973. Contrasts in tectonic evolution of orogenic belts in the southwest Pacific. Journal of the Royal Society of New Zealand 3, 333–362.

Klepeis, K.A., 1994. The Magallanes and Deseado fault zones: Major segments of the South American-Scotia transform plate boundary in southernmost South America, Tierra del Fuego. Journal of Geophysical Research 99 (B11), 22,001–22,014.

Kranck, E.H., 1932. Geological investigations in the Cordillera of Tierra del Fuego. Acta Geographica 4 (2), 231.

Leake, B.E., Woolley, A.R., Arps, C.E.S., Birch, W.D., Gilbert, M.C., Grice, J.D., Hawthorne, F.C., Kato, A., Kisch, H.J., Krivovichev, V.G., Linthout, K., Laird, J., Mandarino, J.A., Maresch, W.V., Nickel, E.H., Rock, N.M.S., Schumacher, J.C., Smith, D.C., Stephenson, N.C.N., Ungaretti, L., Whittaker, E.J.W., Youzhi, G., 1997. Nomenclature of amphiboles: Report of the Subcommittee on Amphiboles of the International Mineralogical Association, Commission on New Minerals and Mineral Names. American Mineralogist 82, 1019–1037.

Liegeois, J.P., Navez, J., Hertogen, J., Black, R., 1998. Contrasting origin of post-collisional high-K calc-alkaline and shoshonitic versus alkaline and peralkaline granitoids, the use of sliding normalization. Lithos 45, 1–28.

Livermore, R., Eagles, G., Morris, P., Nankivell, A., 2004. South America-Antarctica plate motion and tectonics of the southernmost Andes, Scotia Sea and Antarctic Peninsula. In: Carcione, J., Donda, F., Lodolo, E. (Eds.), International Symposium on the Geology and Geophysics of the Southernmost Andes, the Scotia Arc and

the Antarctic Peninsula (GeoSur). Buenos Aires, Argentina (Bolletino di Geofísica Teorica ed Applicata, 45(2), 66–68).
MacDonald, G.A., 1968. Composition and origin of Hawaiian lavas. In: Coats, R.R., Hay, R.L., Anderson, C.A. (Eds.), Studies in Volcanology: A Memoir in Honour of Howel Williams. GSA Mem., vol. 116, pp. 477–522.
Martin, M., Pankhurst, R.J., Fanning, C.M., Thompson, S.M., Calderón, M., Hervé, F., 2001. Age and distribution of plutons across the Southern Patagonian Batholith: New U–Pb data on zircons. In: South American Symposium on Isotope Geology. Sociedad Geológica de Chile, Santiago, pp. 585–588 (Extended Abstracts (CD)).
McKenzie, D., 1985. The extraction of magma from the crust and the mantle. Earth and Planetary Science Letters 74, 81–91.
Morimoto, N., 1988. Nomenclature of pyroxenes. Bulletin de Minéralogie 111, 535–550.
Morrison, G.W., 1980. Characteristics and tectonic setting of the shoshonite rock association. Lithos 13, 97–108.
Mukasa, S.B., Dalziel, I.W.D., 1996. Southernmost Andes and South Georgia Island, North Scotia Ridge: zircon U–Pb and muscovite $^{40}Ar/^{39}Ar$ age constraints on tectonic evolution of southwestern Gondwanaland. Journal of South American Earth Sciences 9 (5–6), 349–365.
Nakamura, N., 1974. Determination of REE, Ba, Fe, Mg, Na and K in carbonaceous and ordinary chondrites. Geochimica et Cosmochimica Acta 38, 757–775.
Nelson, D.R., 1992. Isotopic characteristics of potassic rocks: evidence for the involvement of subducted sediments in magma genesis. Lithos 28, 403–420.
Nelson, E.P., Dalziel, I.W.D., Milnes, A.G., 1980. Structural geology of the Cordillera Darwin – collision-style orogenesis in the southernmost Chilean Andes. Eclogae Geologicae Helvetiae 73-3, 727–751.
Nelson, E., Bruce, B., Elthon, D., Kammer, D., Weaver, S., 1988. Regional lithologic variations in the Patagonian Batholith. Journal of South American Earth Sciences 1 (3), 239–247.
Olivero, E., Martinioni, D., 1996. Late Albian inoceramid bivalves from the Andes of Tierra del Fuego. Age implications for the closure of the Cretaceous marginal basin. Journal of Paleontology 70, 272–274.
Olivero, E., Martinioni, D., Malumián, N., Palamarczuk, S., 1999. Bosquejo geológico de la Isla Grande de Tierra del Fuego, Argentina. In: XIV Congreso Geológico Argentino, Salta. Actas I, pp. 291–294.
Pankhurst, R.J., Riley, T.R., Fanning, C.M., Kelley, S.P., 2000. Episodic silicic volcanism in Patagonia and the Antarctic Peninsula: Chronology of magmatism associated with the break-up of Gondwana. Journal of Petrology 41 (5), 605–625.
Pearce, J.A., 1983. Role of the sub-continental lithosphere in magma genesis at active continental margins. In: Hawkesworth, C.J., Norry, M.J. (Eds.), Continental basalts and mantle xenoliths. Shiva, Nantwich, pp. 230–249.
Petersen, C.S., 1949. Informe sobre los trabajos de relevamiento geológicos efectuados en Tierra del Fuego entre 1945 y 1948. Dirección General de Industria y Minería, Bs. As, Unpublished.
Pitcher, W.S., 1993. The Nature and Origin of Granite. Chapman & Hall, London. 321p.
Quartino, B.J., Acevedo, R., Scalabrini Ortiz, J., 1989. Rocas eruptivas volcanógenas entre Monte Olivia y paso Garibaldi, isla Grande de Tierra del Fuego. Revista de la Asociación Geológica Argentina 44 (1–4), 328–335.
Rickwood, P.C., 1989. Boundary lines between petrologic diagrams which use oxides of major and minor elements. Lithos 22, 247–263.
Schmidt, M., 1992. Amphibole composition in tonalite as a function of pressure: an experimental calibration of the Al-in-hornblende barometer. Contributions to Mineralogy and Petrology 110, 304–310.
Soffia, J.M., 1988. Evaluación geológica y petrolera del sector sur de la provincia de Última Esperanza. Empresa Nacional del Petróleo, Magallanes, Chile, Internal Report 1.011.0252, 89p.
Stern, C.R., 1991. Isotopic composition of late Jurassic and early Cretaceous mafic igneous rocks from the southernmost Andes: implications for sub-Andean mantle. Revista Geológica de Chile 18, 15–23.
Stern, C.R., Saul, S., Skewes, M.A., Futa, K., 1989. Garnet peridotite xenoliths from the Pali-Aike basalts of southernmost South America. In: Kimberlites and Related Rocks. Geological Society of Australia, Special Publication No. 14, vol. 2. Blackwell, Carlton, Australia, pp. 735–744.
Stern, C.R., Frey, F.A., Futa, K., Zartman, R.E., Peng, Z., Kyser, T.K., 1990. Trace-element and Sr, Nd, Pb and O isotopic composition of Pliocene and Quaternary alkali basalts of the Patagonian plateau lavas of the southernmost South America. Contributions to Mineralogy and Petrology 104, 294–308.
Stern, C.R., Mohseni, P., Fuenzalida, R., 1991. Petrochemistry and tectonic significance of Early Cretaceous Barros Arana Formation basalts, southernmost Chilean Andes. Journal of South American Earth Sciences 4 (4), 331–342.
Stille, P., Oberhansli, R., Wenger-Schenk, K., 1989. Hf–Nd and trace element constraints on the genesis of alkaline and calc-alkaline lamprophyres. Earth and Planetary Science Letters 96, 209–219.
Suárez, M., 1976. The Geology of the Southern Andes. Ph.D. Thesis, University of Birmingham, England, 222p.
Suárez, M., 1977. Notas geoquímicas preliminares del Batolito Patagónico al sur de Tierra del Fuego, Chile. Revista Geológica de Chile 4, 15–33.
Suárez, M., 1978. Geología del área al sur del Canal Beagle, región Magallanes y Antártica chilena. Carta Geológica de Chile 1:500.000. Instituto de Investigaciones Geológicas, Santiago de Chile. 48p..
Suárez, M., Pettigrew, T.H., 1976. An upper Mesozoic island-arc back-arc system in the southern Andes and South Georgia. Geological Magazine 113, 305–400.
Suárez, M., Puig, A., Hervé, M., Piraces, R., Cepeda, A., 1979. Geología de la región al sur de los canales Beagle y Ballenero, Andes del Sur, Chile. Nota preliminar. In: II Congreso Geológico Chileno. Arica (Actas 2(4), j19–j28).
Suárez, M., Hervé, M., Puig, A., 1985a. Plutonismo diapírico del Cretácico en Isla Navarino. In: IV Congreso Geológico Chileno. Antofagasta, vol. 4, pp. 549–563.
Suárez, M., Hervé, M., Puig, A., 1985b. Basic magmas in the early evolution of the southernmost Patagonian Batholith, Chile. Geologische Rundschau 74 (2), 337–342.
Suárez, M., Hervé, M., Puig, A., 1985c. Hoja Isla Hoste e islas adyacentes, XII Región. Carta Geológica de Chile 1:250.000, No. 65. Servicio Nacional de Geología y Minería, 113p.
Suárez, M., Puig, A., Hervé, M., 1986. K-Ar dates on granitoids from Archipiélago Cabo de Hornos, southernmost Chile. Geological Magazine 123 (5), 581–584.
Taylor, S.R., McLennan, S.M., 1985. The Continental Crust its Composition and Evolution. Blackwell, Oxford. 312p.
Thompson, R.N., Fowler, M.B., 1986. Subduction-related shoshonitic and ultrapotassic magmas, a study of Siluro-Ordovician syenites from the Scottish Caledonides. Contributions to Mineralogy and Petrology 94, 507–522.
Thompson, R.N., Leat, P.T., Dickin, A.P., Morrison, M.A., Hendry, G.L., Gibson, S.A., 1989. Strongly potassic mafic magmas from lithospheric mantle sources during continental extension and heating evidence from Miocene minettes of northwest Colorado, USA. Earth and Planetary Science Letters 98, 139–153.
Vernon, R.H., 1990. Crystallisation and hybridism in microgranitoid enclave magmas, microstructural evidence. Journal of Geophysical Research 95 (B11), 17849–17859.
Vernon, R.H., 1991. Interpretation of microstructures of microgranitoid enclaves. In: Didier, J., Barbarin, B. (Eds.), Enclaves and Granite Petrology. Developments in Petrology, vol. 13. Elsevier, Englewood Cliffs, NJ, USA, pp. 277–292.
Weaver, S.G., Bruce, R., Nelson, E.P., 1988. Petrology and geochemistry of the Patagonian Batholith, 48°S, Chile. In Geological Society of America 1988 Centennial Celebration, Anonymous (Abstracts with Programs – Geological Society of America, 20(7), 72–73).
Weaver, S.G., Bruce, R., Nelson, E.P., Brueckneer, H.K., LeHuray, A.P., 1990. The Patagonian batholith at 48°S latitude, Chile: Geochemical and isotopic variations. In: Kay, S.M., Rapela, C.W. (Eds.), Plutonism from Antarctica to Alaska, Geological Society of America Special Paper 241. Boulder, Colorado, pp. 33–50.
Winn Jr., R.D., Dott Jr., R.H., 1978. Submarine-fan turbidities and resedimented conglomerates in a Mesozoic arc-rear marginal basin in southern South America. In: Stanley, D.J., Kelling, G. (Eds.), Sedimentation in Submarine Canyons Fans and Trenches. Dowden, Hutchinson and Ross, Stroudsberg, Pennsylvania, pp. 362–373.
Zack, T., Brumm, R., 1998. Ilmenite/liquid partition coefficients of 26 trace elements determined through ilmenite/clinopyroxene partitioning in garnet pyroxene. In: Gurney, J.J., Gurney, J.L., Pascoe, M.D., Richardson, S.H. (Eds.), Seventh International Kimberlite Conference. Red Roof Design, Cape Town, pp. 986–988.
Zen, E., Hammarstrom, J.M., 1984. Magmatic epidote and its petrologic significance. Geology 12, 515–518.